Proceedings of the XXXI International School of Semiconducting Compounds, Jaszowiec 2002

Electronic Structure and Optical Properties of $GaAs_{1-x}N_x$ and $Ga_{1-x}B_xAs$ Alloys

N. Gonzalez Szwacki[a,*], P. Bogusławski[a], I. Gorczyca[b], N.E. Christensen[c] and A. Svane[c]

[a]Institute of Physics, Polish Academy of Sciences
al. Lotników 32/46, 02-668 Warsaw, Poland
[b]High Pressure Research Center, Polish Academy of Sciences
02-480 Warsaw, Poland
[c]Institute of Physics and Astronomy, University of Aarhus
8000 Aarhus, Denmark

The electronic band structure of $GaAs_{1-x}N_x$ ($x = 0.016$ and 0.031) and $Ga_{1-x}B_xAs$ ($x = 0.031$) is studied by *ab initio* calculations using a supercell approach. Based on *ab initio* calculations and group theory we present a comprehensive analysis of the electronic structure of GaAs:N and GaAs:B alloys. In particular, we study the effective mass of conduction electrons in GaAs:N as a function of pressure and the Fermi energy. We find that the lowest conduction band is strongly non-parabolic, which leads to an increase in the effective mass with the electron energy. The rate of the increase is enhanced by the hydrostatic pressure. Theoretical results are compared to experimental data, and a qualitative agreement is found.

PACS numbers: 71.20.Nr, 78.20.Bh

1. Introduction

$GaAs_{1-x}N_x$ and $In_yGa_{1-y}As_{1-x}N_x$ alloys are both promising materials for applications in fabrication of lasers and solar cells, and very interesting from the scientific point of view due to their peculiar properties. The most important features observed in the typical nitrogen concentration regime ($x = 0.005$ to 0.03) are

*corresponding author; e-mail: ngonz@ifpan.edu.pl

the following: (i) an unexpected strong reduction of the band gap [1–7]; this indicates a strongly non-linear dependence of the band gap on the alloy composition (bowing), since the band gap of GaN is larger than that of GaAs by 2 eV, (ii) a much weaker, sublinear pressure dependence of the band gap with a tendency to saturate at high pressures [2, 4, 8], (iii) a high value of the electron effective mass, which increases further as the Fermi energy moves higher into the conduction band [5, 9], (iv) a new optical transition detected by electro-reflectance measurements in samples with $x \geq 0.008$, called E_+, situated about 0.4–0.8 eV (depending on N-content) above the fundamental band gap E_0. While the energy of the band gap decreases with x, the energy of E_+ increases with x [2, 3, 6].

Recently, GaAs with 1–3 atomic percent of boron (and the lattice constant matched to GaAs) has been examined [10, 11] as another candidate for infrared applications. Since B, like N, belongs to the second row of the Periodic Table, a comparable B-induced impact on the electronic structure could be expected. However, the experiment [10, 11] has revealed that this is not the case: the B-induced reduction of the band gap is small, and the pressure dependence of the band gap is almost linear up to 6 GPa and close to that of pure GaAs.

To understand differences between the two alloys, we have performed *ab initio* calculations of their electronic structures. We have analyzed three issues investigated experimentally in detail, namely (i) the dependence of band gaps on the chemical composition and (ii) on hydrostatic pressure, as well as (iii) the electron effective mass. The first experimental values for the electron effective mass have been obtained recently [5, 9, 12], showing an increase in m^* with an addition of nitrogen. There is no direct experimental determination of the electron effective mass for GaAs:N alloys under pressure. In the present work we investigate m^* as a function of pressure and the nitrogen content by means of *ab initio* theory.

2. Methods of calculations

The calculations have been performed using two approaches: quantum molecular dynamics [13, 14] with standard pseudopotentials [15] and the full-potential version of the linear-muffin-tin-orbital method (LMTO). We have used LMTO basis sets including partial waves of s, p, and d character on each atomic site, giving a total of 44 LMTO orbitals per GaAs unit cell. In the case of the molecular dynamics approach the cutoff energy of 30 Ry for the plane wave basis set was sufficient to obtain convergent results. In both cases we have used large unit cells with 64 and 128 atoms; with this choice the substitution of one host atom by B or N corresponds to the alloy compositions of 3.1% and 1.6%, respectively. The experimental lattice constants of the end compounds were assumed, together with the alloy lattice constants chosen according to Vegard's law. The pressure dependence of the lattice constants was calculated based on Murnaghan equation of state. Compared to experiment, the values of the band gaps of GaAs at Γ, L, and

X are underestimated by almost the same amount, 0.6 eV, which is a well-known consequence of the local density approximation (LDA) that we use. Moreover, the LDA gap errors are k-dependent, and this usually leads to errors in the derived effective masses. In GaAs this error is particularly large at the minimum of the conduction band (at the Γ point), see for example Ref. [16]. On the other hand, it was shown that the pressure coefficients of the band gaps and of the effective mass are well predicted by LDA [16–18]. Although we do not obtain the proper absolute values of the electron effective mass, we may still examine the trends in its pressure and composition dependence. Similarly, the momentum matrix elements are expected to be well described.

3. Electronic structure of GaAs:N and GaAs:B

The calculated lattice constants of pure end compounds are 5.56, 4.48, and 4.72 Å for GaAs, GaN, and BAs, respectively. These values are smaller than the experimental ones by about 2 per cent, which is a typical error due to the use of the local density approximation. On the other hand, the calculated lattice constants of the investigated alloys satisfy Vegard's law. In Fig. 1 we present the total energy

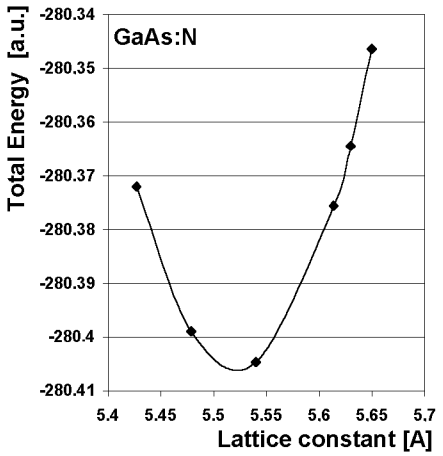

Fig. 1. Total energy plotted as a function of the lattice constant for GaAs:N with 3% of N.

as a function of the lattice constant for GaAs:N alloy with 3% of N. The obtained value of 5.523 Å for the equilibrium lattice constant is very close to the value expected from Vegard's law, 5.527 Å. A similar accuracy is obtained for GaAs:B.

We now turn to the composition dependence of the energy gap at the Γ point. The results are presented in Fig. 2. As we can see, doping of GaAs with N induces a strong reduction of the band gap. For GaAs with 3% of nitrogen, the

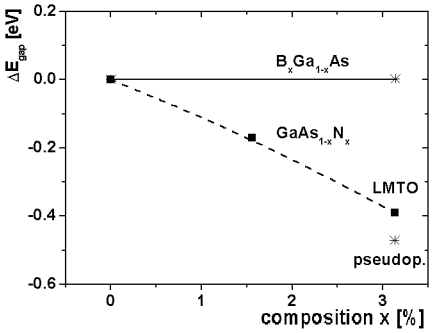

Fig. 2. Composition dependence of the energy gap for GaAs with N and B. The squares and the stars denote results obtained while using LMTO and the pseudopotential method, respectively.

reduction of the band gap obtained using two different methods of calculation, LMTO and the pseudopotential approach, 0.39 eV and 0.47 eV, are close. The average value, 0.43 eV, is in good agreement with the experimental one, ~ 0.5 eV. For the composition $x = 0.016$, the calculated reduction of the band gap, 0.17 eV, is somewhat smaller than the experimental value of 0.26 eV. The impact of 3% of B in GaAs is clearly less pronounced, because the calculated energy gaps of GaAs and GaAs:B are the same within the accuracy of our calculations. This result is in good agreement with experiment, since the observed increase in E_0 induced by 3% is only 0.02 eV. However, this result implies that there is a very pronounced bowing of the band gap. In fact, we find the reduction of E_0 by 0.11 eV relative to the linear interpolation between the energy gaps of GaAs and BAs. Differences between the behavior of the $\Delta E_{\rm gap}$ for B and N stem from the different impact of atomic relaxation on the electronic structure [19].

In Fig. 3 we present the calculated dispersion of conduction bands of $GaAs_{1-x}N_x$ (solid line) for the composition $x = 0.03$ at zero pressure. For comparison, we also present the electronic structure of pure GaAs (dashed line). The figure shows that in the presence of N there is a decrease in the band gap by 0.39 eV with respect to pure GaAs. In the supercell approach that we use, we can investigate the behavior of the secondary conduction minima from the L and X points of the zinc blende Brillouin zone (BZ), which now are at the Γ point of the folded BZ. We can see that the impurity potential splits the fourfold degenerate L-derived state into a singlet, $a_1(L_{1c})$, lying below, and the triplet, $t_2(L_{1c})$, lying slightly above the unperturbed host state. The calculated value of the splitting is 0.18 eV for $x = 0.031$ (and 0.14 eV for $x = 0.016$). The presence of the impurity potential also induces a splitting of the X_{1c}-derived conduction state. The lowest X conduction levels in GaAs:N gives rise to a singlet $a_1(X_{1c})$, and a doublet $e_2(X_{1c})$. The energy splitting, 0.15 eV, is comparable with the splitting at L. For the lower composition $x = 0.016$ the splitting of X_{1c} is smaller, 0.05 eV.

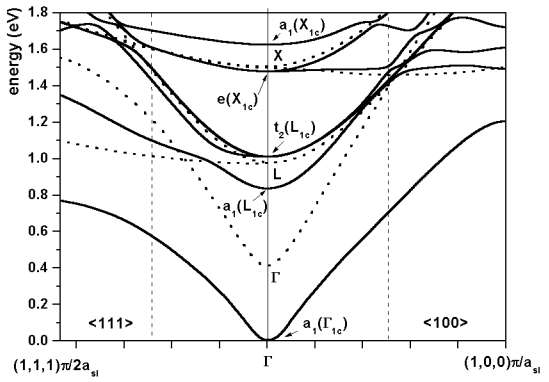

Fig. 3. Band structure for wave vectors along the (111) and the (100) directions of $GaAs_{1-x}N_x$ for $x = 0.031$ (solid lines) and GaAs (dashed lines). The vertical dashed lines indicate the range of wave vectors corresponding to the electron concentrations covered in Fig. 5. The point $(1,1,1)\pi/2a_{sl}$ is only halfway towards the Brillouin zone edge, where a_{sl} is the supercell lattice constant, twice larger than that of GaAs.

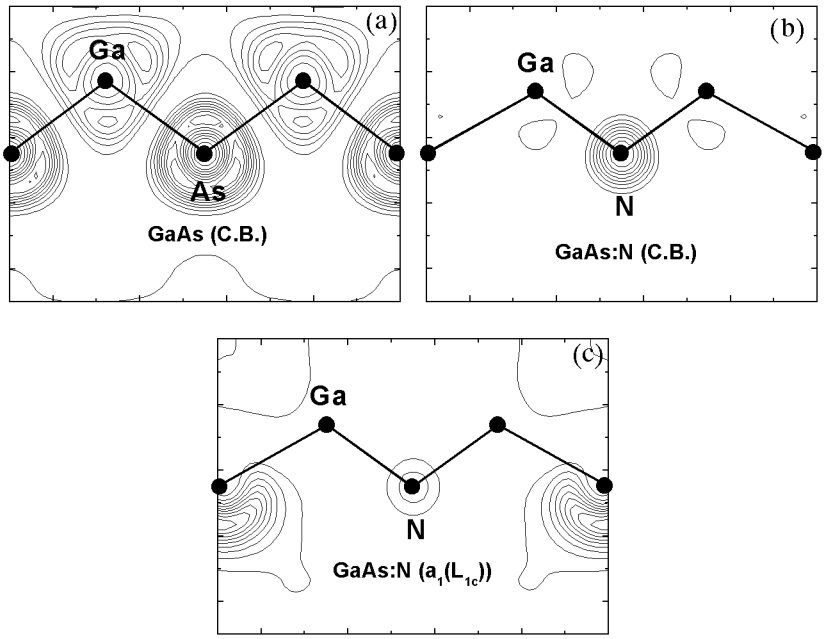

Fig. 4. Wave function (a) of the bottom of the conduction band of pure GaAs, (b) of the bottom of the conduction band of GaAs:N with 3% of N, and (c) of the second conduction band $a_1(L_{1c})$ in GaAs:N.

In Fig. 4 we show the wave functions of three conduction states. The bottom of the conduction band of pure GaAs, and of GaAs:N doped with 3% of nitrogen,

are shown in Figs. 4a and b, respectively. Both wave functions are antibonding combinations of s(cation) and s(anion) orbitals. As it is seen in Fig. 4b, in the presence of impurities there is a strong localization of the bottom of the conduction band on N atoms. We have quantitatively analyzed this effect by projecting the wave functions on the atomic orbitals. In pure GaAs, the bottom of the conduction band contains 49% of s(Ga) and 51% of s(As); this feature is seen in Fig. 4a. Consequently, considering the unit cell with 64 atoms we find that the contribution of each cation and anion atom to the bottom of the conduction band of GaAs is 1.5%. In the case of GaAs:N, we find that the contribution of s(N) to the bottom of the conduction band, equal to 12%, is almost an order of magnitude higher, which agrees with Fig. 4b. A comparable but weaker localization of the conduction band occurs also in GaAs:B; in this case, the contribution of s(B) to the bottom of the conduction band is equal to 7%. The wave function of the second conduction state in GaAs:N, which is responsible for the E_+ transition, is shown in Fig. 4c. We see that this state, which is induced by the presence of N, is clearly *not* localized on N, but rather on its third neighbors. Finally, we notice that the admixture of the s(impurity) orbitals to higher conduction states is negligible, with one exception of a conduction state in GaAs:B located 1.2 eV above the bottom of the conduction band, which contains 9% of B orbitals.

In the presence of the impurity potential there is a coupling between the states derived from Γ, L, and X points of the BZ which have the same symmetry. This interaction is responsible for many unusual properties of both GaAs:N and GaAs:B alloys. One of them is a nonlinear dependence of the energy gap on hydrostatic pressure. The effect takes place in both alloys, but the non-linearity is less pronounced in the case of B [19]. The impurity-induced coupling of states can be analyzed in the reciprocal space by projecting the states of the alloy onto the states of pure GaAs. From the analysis of the wave function for the Γ-, L- and X-derived states we obtain that the bottom of the conduction band $a_1(\Gamma_{1c})$ contains a strong admixture of the $a_1(L_{1c})$ state, which is 20% and 31% for B and N, respectively. The contribution of X_{1c}, about 2%, is an order of magnitude smaller, indicating a weak Γ_{1c}–X_{1c} interaction in both alloys at zero pressure. Consequently, for lower pressures the non-linearity is due to the coupling between the bottom of the conduction band $a_1(\Gamma_{1c})$ and the $a_1(L_{1c})$ state. For higher pressures, the effect stems from the increasing coupling between $a_1(\Gamma_{1c})$ with the singlet $a_1(X_{1c})$, which adds to the non-linearity of the pressure dependence of the band gap. For pressures greater than 8 GPa, the character of the bottom of the conduction band is dominated by the contribution from the X_{1c} state. This agrees with the experimentally observed pressure dependence of the fundamental transition E_0. We also notice that the second conduction state $a_1(L_{1c})$, which, according to our previous calculations [19], is the final state of the transition E_+, also exhibits a strongly non-linear pressure dependence. Finally, in the case of GaAs:B alloy, there is a change of the character of the band gap from direct to indirect at ~ 6 GPa, which

does not occur in GaAs:N alloys [19]. Differences between the impact of N and B on the pressure behavior of E_{gap} stem from the different substitution site of the host atom and could be explained on the base of the group theory [19].

As a result of the $\Gamma-L-X$ coupling discussed above, the pressure coefficients of the band gaps of alloys are smaller than those of pure GaAs. More specifically, we find that for pure GaAs, the calculated coefficients of the band gaps at the Γ, L, and X points are equal to 110 meV/GPa, 40 meV/GPa, and –20 meV/GPa, respectively. In the limit of low pressure, the pressure coefficient obtained for $\mathrm{GaAs}_{1-x}\mathrm{N}_x$ is 63 meV/GPa for $x = 0.016$, and 55 meV/GPa for $x = 0.031$. As we can see, the influence of the L_{1c} state on the bottom of the conduction, and therefore on the pressure coefficient of the band gap, increases with the increasing content of N. (For the sake of completeness, we also give the corresponding values of deformation potentials, which are 8.5, 6.8, and 4.6 eV for GaAs, GaAs:B, and GaAs:N, respectively.)

4. Effective mass of conduction electrons in GaAs:N

For the electronic effective mass calculations we have performed band structure calculations of $\mathrm{GaAs}_{1-x}\mathrm{N}_x$ for a few values of the hydrostatic pressure (0.0, 2.8, 6.4, and 8.5 GPa) and two values of x (0.016, 0.031). We have found a strong non-parabolicity of the lowest conduction band of GaAs:N. In order to quantify this effect we calculated the k-dependence of the effective mass, $m^*(k)$, according to

$$\frac{1}{m^*(k)} = (\hbar^2 k)^{-1} \frac{\mathrm{d}E}{\mathrm{d}k}.$$

Figure 5 shows the variation of m^* with electron concentration $n_{\mathrm{e}}(k_{\mathrm{F}})$ which is related to the Fermi radius, k_{F}, through $n_{\mathrm{e}}(k_{\mathrm{F}}) = k_{\mathrm{F}}^3/3\pi^2$. In Fig. 5a we com-

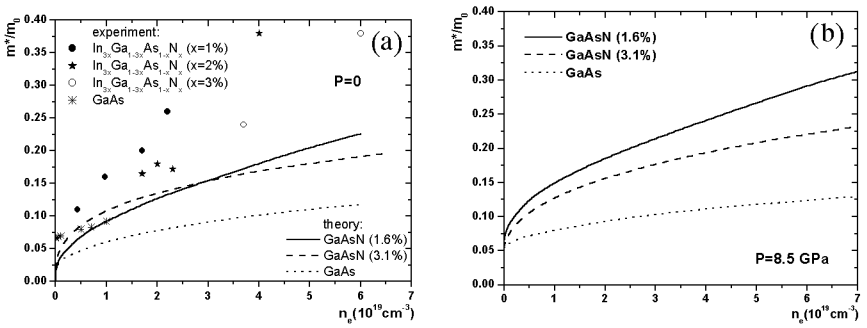

Fig. 5. The calculated electron effective mass of $GaAs_{1-x}N_x$ for $x = 0.016$ (solid line), $x = 0.031$ (dashed line), and of GaAs (dotted line) as a function of electron concentration in comparison with experiment (points); (a) $P = 0$, (b) $P = 8.5$ GPa.

pare the dependence of electron effective masses on electron concentration (Fermi energy) as determined experimentally for $In_{3x}Ga_{1-3x}As_{1-x}N_x$ (for $x = 0.01, 0.02$, 0.03) and theoretically for $GaAs_{1-x}N_x$ (for $x = 0.016$, 0.031), as well as for pure GaAs. We observe that although the calculated masses are too small, the general shape of the n_e-dependence of m^* is very similar to the experimental one, especially for low values of n_e. The dashed and full-line curves in Fig. 5a ($P = 0$) intersect at $n_e \approx 2.5 \times 10^{19}$ cm^{-3}, i.e., for low electron concentrations the mass in the compound with the *high* N concentration is larger than the mass in the dilute compound, whereas the opposite takes place for samples with higher electron concentrations. It is not possible to decide whether the experiments confirm this relationship since there are too few data points (Fig. 5a), but the experimental values of m^* for $x = 0.03$ are indeed lower than those for $x = 0.01$ and 0.02. The calculations show that the crossing point of the two curves moves towards $n_e = 0$ as the pressure is applied, disappearing at $P = 2.8$ GPa. Figure 5b shows the calculated masses as a function of n_e for $P = 8.5$ GPa. In that case, the effective mass in the compound with the *high* N concentration is smaller than the mass in the more diluted compounds for the whole range of the electron concentrations. Comparing Figs. 5a and b we observe that generally the effective mass increases with pressure, this being more pronounced for a lower nitrogen concentration.

In the case of pure GaAs, the effective mass of conduction electrons is determined by the $k \cdot p$ coupling between the light hole band and the conduction band. Within the $k \cdot p$ approach, the effective mass is proportional to the band gap. In the case of GaAs:N, there is an additional coupling between the lowest conduction band with the E_+ band. This coupling is responsible for the increase in the effective mass in spite of the decrease in E_0 induced by the presence of the N impurities. In the presence of hydrostatic pressure two effects take place: (i) the increase in the energy gap with pressure, and (ii) the increase in $E_0 - E_+$ coupling due to the decrease in their energy separation. These two features combined explain the observed increase in the effective mass with pressure.

Acknowledgments

The work is partially supported by the State Committee for Scientific Research grant 2 P03B 04719.

References

[1] M. Weyers, M. Sato, *Jpn. J. Appl. Phys., Part 2* **31,** L853 (1992); M. Kondow, K. Uomi, K. Hosomi, T. Mozume, *ibid.* **33,** L1056 (1994).

[2] W. Shan, W. Walukiewicz, J.W. Ager III, E.E. Haller, J.F. Geisz, D.J. Friedman J.M. Olson, S.R. Kurtz, *Phys. Rev. Lett.* **82,** 1221 (1999); W. Shan, W. Walukiewicz, K.M. Yu, J.W. Ager III, E.E. Haller, J.F. Geisz, D.J. Friedman, J.M. Olson, S.R. Kurtz, C. Nauka, *Phys. Rev. B* **62,** 4211 (2000).

[3] J.D. Perkins, A. Mascarenhas, Y. Zhang, J.F. Geisz, D.J. Friedman, J.M. Olson, S.R. Kurtz, *Phys. Rev. Lett.* **82,** 3312 (1999).

[4] E.D. Jones, N.A. Modine, A.A. Allerman, S.R. Kurtz, A.F. Wright, *Phys. Rev. B* **60,** 4430 (1999).

[5] C. Skierbiszewski, P. Perlin, P. Wisniewski, W. Knap, T. Suski, *Appl. Phys. Lett.* **76,** 2409 (2000).

[6] P.J. Klar, H. Grüning, W. Heimbrodt, J. Koch, F. Höhnsdorf, W. Stolz, P.M.A. Vicente, J. Camassel, *Appl. Phys. Lett.* **76,** 3439 (2000).

[7] H.M. Cheong, Y. Zhang, A. Mascarenhas, J.F. Geisz, *Phys. Rev. B* **61,** 13687 (2000).

[8] P. Perlin, S.G. Subramanya, D.E. Mars, J. Kruger, N.A. Shapiro, H. Siegle, E.R. Weber, *Appl. Phys. Lett.* **73,** 3703 (2098).

[9] C. Skierbiszewski, P. Perlin, P. Wisniewski, T. Suski, J.F. Geisz, K. Hingerl, W. Jantsch, D. Mars, W. Walukiewicz, *Phys. Rev. B* **65,** 035207 (2002).

[10] J.F. Geisz, D.J. Friedman, J.M. Olson, S.R. Kurtz, R.C. Reedy, A.B. Swartzlander, B.M. Keyes, A.G. Norman, *Appl. Phys. Lett.* **76,** 1443 (2000).

[11] W. Walukiewicz, private communication.

[12] P.N. Hai, W.M. Chen, I.A. Buyanova, H.P. Xin, C.W. Tu, *Appl. Phys. Lett.* **77,** 1650 (2000).

[13] R. Car, M. Parrinello, *Phys. Rev. Lett.* **55,** 2471 (1985).

[14] C. Wang, Q.-M. Zhang, J. Bernholc, *Phys. Rev. Lett.* **69,** 3789 (1992).

[15] G.B. Bachelet, D.R. Hamann, M. Schluter, *Phys. Rev. B* **26,** 4199 (1982). A soft pseudopotential of N was generated by G. Li, S. Rabii, unpublished.

[16] N.E. Christensen, *Phys. Rev. B* **30,** 5753 (1984).

[17] N.E. Christensen, I. Gorczyca, *Phys. Rev. B* **50,** 4397 (1994).

[18] I. Gorczyca, A. Svane, N.E. Christensen, *Phys. Rev. B* **60,** 8147 (1999).

[19] N. Gonzalez Szwacki, P. Bogusławski, *Phys. Rev. B* **64,** R161201 (2001).